



PERGAMON

Deep-Sea Research II 48 (2001) 457–482

DEEP-SEA RESEARCH
PART II

www.elsevier.com/locate/dsr2

A 3-D prognostic numerical model study of the Georges bank ecosystem. Part II: biological–physical model[☆]

Peter J.S. Franks^{a,*}, Changsheng Chen^b

^a*Marine Life Research Group, Scripps Institution of Oceanography, University of California, San Diego, La Jolla, CA 92093-0218, USA*

^b*Department of Marine Sciences, The University of Georgia, Athens, GA 30602-2206, USA*

Received 10 December 1998; received in revised form 25 August 1999; accepted 22 December 1999

Abstract

A three-dimensional ecosystem-physical model is presented for the Gulf of Maine (GOM), including Georges Bank (GB) and the Nantucket Shoals (NS). The coupling of a simple nutrient-phytoplankton-zooplankton model to a detailed physical model forced by the M_2 tides generated patterns of plankton and nutrients that agreed closely with data. High phytoplankton biomass developed in regions of strong vertical mixing, particularly on GB and the eastern flank of the NS. Low concentrations were seen in the GOM, where a subsurface chlorophyll maximum developed at 20 m, coincident with the top of the nutricline. High surface phytoplankton concentrations in the GOM, and low concentrations on the top of GB led us to reject several parameterizations of the biological model. A horizontally dependent euphotic depth was required for an accurate simulation of GB and the GOM with a single biological parameter set. High f -ratios developed in the frontal regions, implying a vertical flux of nutrients from below the euphotic zone. Biological patterns were dominated by vertical mixing induced by the tidal forcing, though removing advection from the simulations led to a decrease in the regions of high f -ratio. A surprising feature of the model was the robustness of the simulated patterns of phytoplankton and nutrients, in spite of large changes in biological parameters and the removal of advection from the model. This reinforces the hypothesis of the overall dominance of vertical mixing in structuring the plankton in and around GB. © 2000 Elsevier Science Ltd. All rights reserved.

1. Introduction

The cod fishery of the Gulf of Maine (GOM), Georges Bank (GB) and the Grand Banks was central to the economic, social and cultural development of New England and Eastern Canada

[☆] Paper published in December 2000.

* Corresponding author. Tel.: + 1-858-534-7528; fax: + 1-858-822-0562.

E-mail addresses: pfranks@ucsd.edu (P.J.S. Franks), chen@whale.marsci.uga.edu (C. Chen).

(Kurlansky, 1998). Fluctuations in the cod stocks reverberated throughout the region, with low catches leading to unemployment and regionally depressed economies. A focus of the US GLOBEC GB program is to understand the links between climate change and changes in the recruitment of cod and haddock on GB. One link in this chain is to understand the couplings between climate forcing and primary production in this region.

One approach to achieving a better understanding of the dynamics controlling primary and secondary production on GB and in the GOM is to develop models of these processes. These models can be used to test hypotheses otherwise not amenable to testing in the field. Several such models have been developed to investigate the biological–physical couplings on GB. These have been well reviewed by Lynch et al. (1998), who present one of the most sophisticated models yet applied to this region for the study of *Calanus finmarchicus* dynamics. Previous modelling efforts of the entire ecosystem on GB and the GOM have been few, however. Klein (1987) and Lewis et al. (1994) both presented simple ecosystem models in idealized geometries representing GB, forced by a kinematic anticyclonic gyre (Klein), or strong wind events applied to a detailed three-dimensional (3D) circulation model (Lewis et al., 1994). Neither of these models included tides or the details of tidally driven mixing.

Franks and Chen (1996) (denoted FC96) coupled a simple nutrient–phytoplankton–zooplankton (NPZ) model to a detailed, two-dimensional (2D) prognostic model of a cross-section through GB (Fig. 1, Section A), forced with the M_2 tide. They used this model to explore the influence of tidally generated mixing and advection on the development of patterns in the summertime plankton community on GB and its surrounding fronts. The model produced cross-frontal patterns of nutrients and plankton that were in close quantitative agreement with data from GB. Strong vertical mixing on the top of GB homogenized the plankton there. An abrupt change in pattern was seen at the fronts separating the stratified waters offshore, and the well-mixed waters on GB. Asymmetric patterns of tidal mixing over a tidal cycle at the fronts led to cross-frontal fluxes of nutrients. These fluxes supported enhanced primary production in the fronts, leading to the formation of subsurface patches of phytoplankton at the fronts — a feature often seen at tidal fronts. The simulated patterns of plankton and their trophic fluxes (uptake, regeneration, etc.) agreed well with data of Horne et al. (1989) from GB. In spite of the good agreement of the model and data on GB, the patterns were less successfully simulated off the bank.

In the present study, we expand on FC96, and present a 3D biological–physical model of the entire GOM, including GB. There are a great many details to consider when formulating and running such a model; here we explore a small subset of the possible variations. Our fundamental question is:

“Can the nutrients, phytoplankton and zooplankton fields on GB be modelled as a physically driven perturbation of the biology in the GOM?”

We begin by developing a physical–biological model that gives an accurate simulation of the biological patterns in the central GOM. We then explore how well this model matches the biological patterns on GB, testing the hypothesis that the plankton and nutrient patterns on GB are a physical perturbation of the patterns in the GOM. We also explore the relative importance of mixing and advection in the generation of these biological patterns. We show that the plankton patterns on GB can be reasonably simulated as a physical perturbation of the GOM state, though a horizontally depth-dependent euphotic depth was necessary to obtain the best agreement with

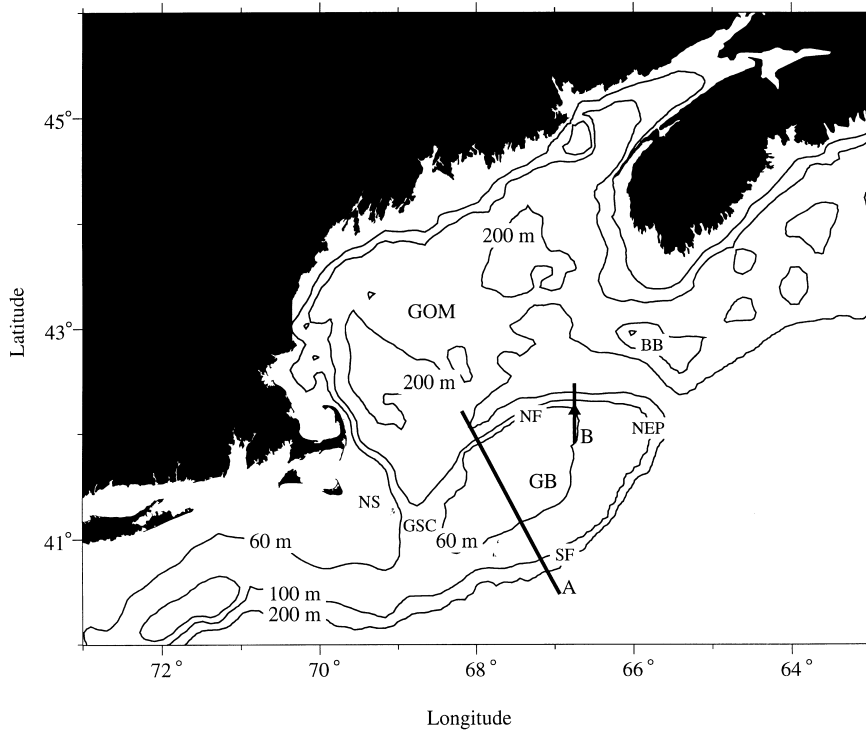


Fig. 1. Map of the Gulf of Maine (GOM), including Georges Bank (GB); the Nantucket Shoals (NS); the Northern Flank (NF), Southern Flank (SF), and North-East Peak (NEP) of Georges Bank; the Great South Channel (GSC); and Brown's Bank (BB). Section A indicates the location of the 2D cross-bank section described in the text, while Section B corresponds to the transect of Horne et al. (1989). The large triangle on Section B gives the location of the mooring data.

data. The biological patterns are strongly determined by vertical mixing, though advective processes are necessary for an accurate simulation of the extent of the frontal zones, and the vertical transport of nutrients to the euphotic zone.

2. Physical model

The following description of the physical model is excerpted from the companion paper, Chen et al. (2000). A more extensive description can be found in that paper. The numerical model used in this study is a modified version of the 3D coastal ocean circulation model developed originally by Blumberg and Mellor (1987) (the ECOM-si model). The model incorporates the Mellor and Yamada (1974, 1982) level 2.5 turbulent closure scheme (as modified by Galperin et al., 1988) to provide a time- and space-dependent parameterization of vertical turbulent mixing. The basic semi-implicit model was described in detail by Blumberg (1994) and briefly in Chen et al. (2001).

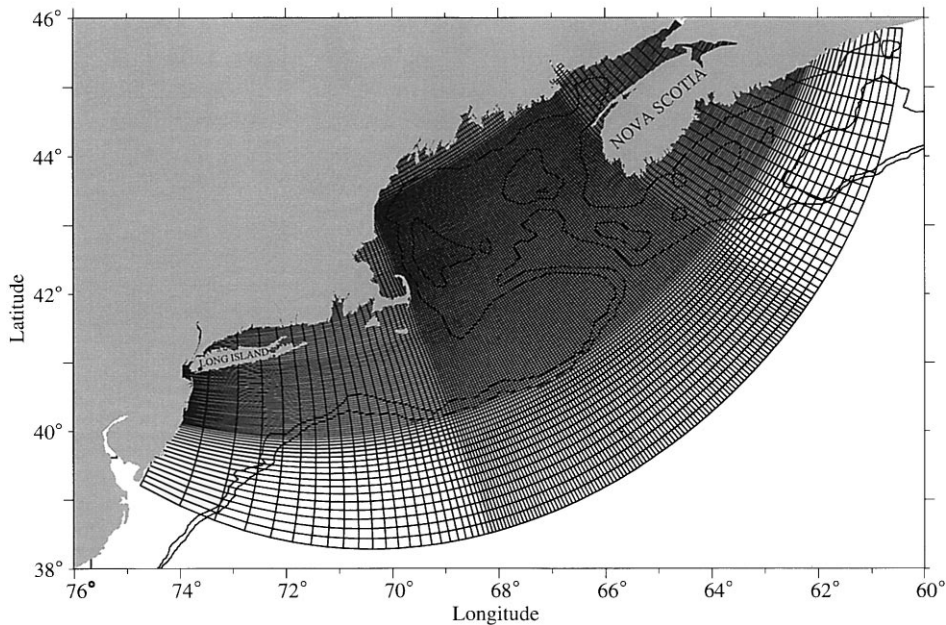


Fig. 2. Horizontal model grid.

The numerical domain covered the GOM/GB region and was enclosed by an open boundary running from the New Jersey shelf to the Nova Scotia shelf (Fig. 2). The numerical grid utilized orthogonal curvilinear coordinates in the horizontal and a σ -coordinate in the vertical, with enhanced horizontal resolution over the GOM/GB. Horizontal resolution varied from 1.5–3 km over GB and the interior region of the GOM, to 4–20 km near the open boundary. Thirty-one uniform σ -levels were used in the vertical, corresponding to a vertical resolution of 4–1.3 m over GB, and ~ 10 m offbank. The bottom depths at each grid in the model were interpolated directly from the new geometric data set of GOM/GB with a 1 km horizontal resolution. The model time step was 414 s, resulting in 108 time steps over an M_2 (12.42 h) tidal cycle.

The model was forced along the open boundary by the barotropic M_2 tidal elevation and phase taken from the global $0.5^\circ \times 0.5^\circ$ inverse tidal model of Egbert et al. (1994). A gravity wave radiation condition for currents was applied at the open boundary to minimize energy reflection into the computational domain.

To facilitate the comparison with the 2D model results of FC96, we ran the 3D model as an initial value problem with early summer stratification. The initial temperature distribution for the early summer stratification case was simply specified by a linear function of z with a value of 15°C at the surface and 6°C at a depth of 300 m. The resulting initial buoyancy frequency N for this case is 10^{-2} s^{-1} , which is typical of summer stratification over GB. The model was run for 20 tidal cycles, by which time it had reached a relatively steady cyclic state. Figures are calculated from the 20th tidal cycle, often averaged over the tidal period.

3. Biological model

The biological model was the simple NPZ model of Franks et al. (1986), as used in FC96. Nitrogen is used as a tracer for the state variables. Dissolved nutrients are taken up by the phytoplankton following Michaelis–Menten kinetics, while phytoplankton are grazed by zooplankton with an Ivlev functional response:

$$\frac{dP}{dt} = \frac{V_m N}{k_s + N} f(I_0, z) P - Z R_m (1 - e^{-\lambda P}) - \varepsilon P, \quad (1)$$

$$\frac{dZ}{dt} = \gamma Z R_m (1 - e^{-\lambda P}) - g Z, \quad (2)$$

$$\frac{dN}{dt} = \frac{V_m N}{k_s + N} f(I_0, z) P + (1 - \gamma) Z R_m (1 - e^{-\lambda P}) + \varepsilon P + g Z, \quad (3)$$

where P is the phytoplankton, Z the zooplankton and N the dissolved nutrient, all in $\mu\text{mol NI}^{-1}$. The total amount of nutrient, N_T , is conserved: $N + P + Z = N_T$.

There are seven parameters governing the Franks et al. (1986) model; values of these parameters are discussed in Franks et al. (1986). The maximal phytoplankton nutrient uptake rate (and growth rate) is V_m , with a half-saturation constant k_s . The zooplankton have a maximal grazing rate R_m , with the grazing efficiency controlled by λ . Only a portion, γ , of the ingested phytoplankton is assimilated by the zooplankton, the remainder being recycled into dissolved nutrients. Both phytoplankton and zooplankton die at rates ε and g , respectively. These dead fractions are immediately recycled into dissolved nutrients. The phytoplankton depend on incident irradiance I_0 through the function $f(I_0, z)$, which we have taken to be linear in I_0 :

$$f(I_0, z) = I_0 e^{-k_{\text{ext}} z} \quad (4)$$

where k_{ext} is the diffuse attenuation coefficient for irradiance and z is depth below the surface. No dependence of k_{ext} on the local particle (phytoplankton) concentration was included. I_0 was a constant in space and time in the following simulations; therefore $f(I_0, z)$ was scaled so that the maximum value was 1 at the surface (i.e., $f(I_0, z) = e^{-k_{\text{ext}} z}$). The justification for the parameter values is given in FC96. Changes to those parameters values in the present simulations are described and justified below.

For comparing the phytoplankton nitrogen concentrations to chlorophyll concentrations, we use a 1:1 mapping of $\mu\text{mol NI}^{-1}$ to $\mu\text{g chl l}^{-1}$. This implies a C:chl ratio of about 80, which is reasonable given the large variation in this value.

The physical and biological fields were coupled in the usual way, with biological fields being advected and diffused by the physical dynamics. The equation for phytoplankton, for example, was

$$\begin{aligned} \frac{\partial P}{\partial t} + u \frac{\partial P}{\partial x} + v \frac{\partial P}{\partial y} + w \frac{\partial P}{\partial z} + w_s \frac{\partial P}{\partial z} = & \frac{\partial}{\partial x} \left(\kappa_x \frac{\partial P}{\partial x} \right) + \frac{\partial}{\partial y} \left(\kappa_y \frac{\partial P}{\partial y} \right) + \frac{\partial}{\partial z} \left(\kappa_z \frac{\partial P}{\partial z} \right) \\ & + \frac{V_m N}{k_s + N} f(I_0, z) P - Z R_m (1 - e^{-\lambda P}) - \varepsilon P. \end{aligned} \quad (5)$$

The ambient physical velocities are u, v and w , while the horizontal and vertical eddy diffusivities are κ_x, κ_y and κ_z , respectively (note that they have spatial dependence). The phytoplankton sink with speed $w_s = 1 \text{ m d}^{-1}$; the other biological fields do not move relative to the water. The equations for the other biological fields were similar, though with different biological dynamics (Eqs. (2) and (3)) and no sinking.

4. Approach

In FC96 we explored the biological dynamics on GB using a 2D physical–biological model based on the same equations as the present study. Since that study concentrated on the bank and the surrounding fronts, biological parameters were chosen to reflect the dominant organisms on the bank: a phytoplankton community composed largely of diatoms, and a zooplankton community with a large fraction of copepods. In the present study, we explore the whole GOM region, of which GB is a part. We therefore wish to obtain a good match of the modelled biological fields with measurements from the relatively quiescent GOM, and explore how these fields become modified on the physically dynamic GB. Our fundamental question is:

“Can the nutrients, phytoplankton and zooplankton fields on GB be modelled as a physically driven perturbation of the biology in the GOM?”

Through a series of case studies, we explore the modifications necessary to allow the simple biological model with a single parameter set to simulate the biological fields in both the GOM and GB:

Case 1: The initial study used the same biological parameters as FC96 (Table 1).

Case 2: A modified set of biological parameters was used to better represent the biological taxa in the GOM (Table 1), including an increase in N_T to reflect the high values of nitrate in the deep waters of the GOM.

Table 1

Parameter values for the various cases of the biological model. The diffuse attenuation coefficient is a function of the water depth h in Case 4, with $f(h) = 0.065 + (0.1 - 0.065)\{1 - \tanh[(h - 80)/40]\}/2$. N_T is a linear function of depth for Cases 2, 4, and 5, and is equal to 15 below 180 m

Parameter	Description	Units	Case 1	Case 2	Case 3	Case 4	Case 5
V_m	Maximum nutrient uptake rate	d^{-1}	2.0	2.0	2.0	2.0	2.0
k_s	Half-saturation constant for nutrient uptake	$\mu\text{mol NI}^{-1}$	1.0	0.1	0.1	0.1	0.1
R_m	Maximum grazing rate	d^{-1}	0.5	0.5	0.5	0.5	0.5
g	Zooplankton death rate	d^{-1}	0.2	0.1	0.1	0.1	0.1
λ	Ivlev constant for grazing	$(\mu\text{mol NI}^{-1})^{-1}$	0.2	0.2	0.2	0.2	0.2
ε	Death rate of phytoplankton	d^{-1}	0.1	0.1	0.1	0.1	0.1
γ	Proportion of assimilated nutrient by zooplankton		0.7	0.7	0.7	0.7	0.7
k_{ext}	Diffuse attenuation coefficient	m^{-1}	0.1	0.09	0.09	$f(h)$	0.09
N_T	Total amount of nutrient	$\mu\text{mol NI}^{-1}$	7.0	10.00	6–0.05z	6–0.05z	6–0.05z

Case 3: The influence of a depth-dependent profile of total nutrient (N_T) was explored using the biological parameters of Case 2.

Case 4: Using the same biological parameters and nutrient profile as Case 3, a horizontally variable diffuse attenuation coefficient was employed to simulate the effects of vertical resuspension of turbid material in shallow waters (on GB and other banks, and in coastal regions). Case 4 gave the best fit to the biological data, and will be described in more detail than the other cases.

Case 5: To explore the importance of advection to the development of the biological fields, the biological parameters and nutrient distribution of Case 3 were used in a simulation with no advection of the biological fields (only vertical mixing). This case can be compared to 1D vertical models of tidally forced regions to assess the importance of 2D and 3D dynamics.

In designing these cases for study, we have purposely kept the biological parameters as global constants, altering only the physical parameters (including the euphotic depth). In all but Case 4, the biological initial condition had no horizontal variability (except where it intersected the

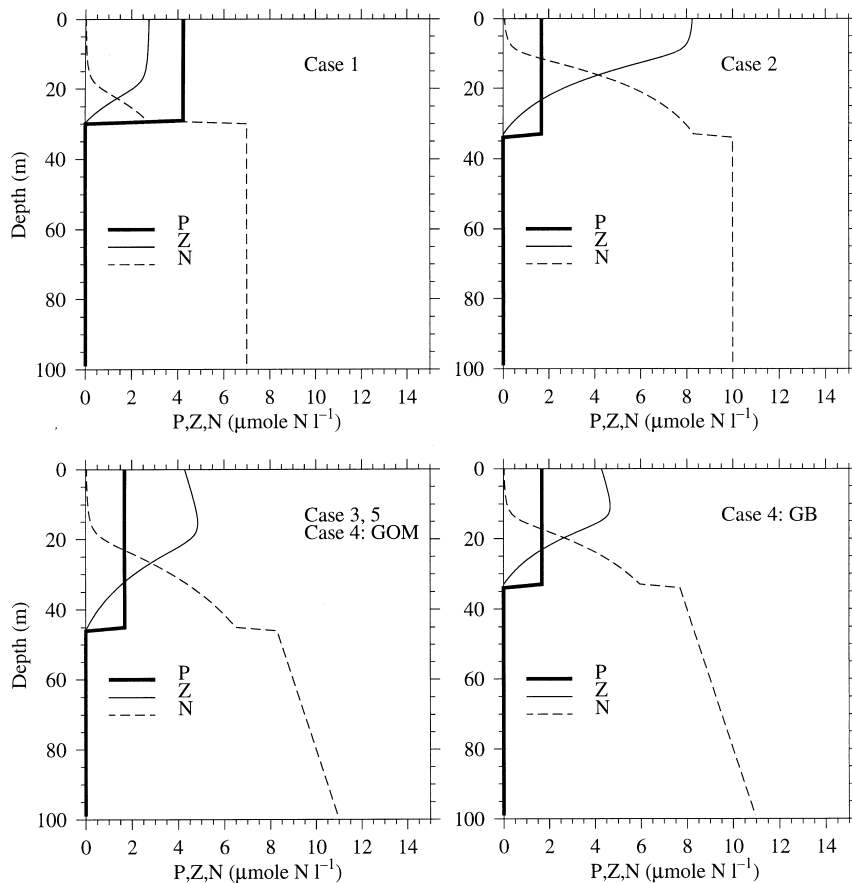


Fig. 3. Vertical profiles of the initial conditions for the biological model.

bottom), thus any horizontal gradients that were generated by the tidal forcing had to have arisen through pure physical forcing, or a biological response to the physical perturbations.

All models were initialized with the biological fields at steady state (as in FC96) (Fig. 3). Thus, any changes to the biological fields resulted from tidal forcings leading to advection, mixing, and changes in the biological couplings resulting from changes in local biomasses and growth rates. Phytoplankton were allowed to sink at 1 m d^{-1} in all cases (see FC96). The tidal forcing is described in Chen et al. (2001).

5. Results

5.1. Physical model

A thorough description of the results of the physical model is given in the companion paper (Chen et al., 2001).

Tidally generated mixing created a well-mixed region on the top of GB, with tidal fronts between the 40 and 60 m isobaths (Fig. 4). Well-mixed regions were also generated on the eastern flank of the Nantucket Shoals (NS), at the southern tip of Nova Scotia, and over Brown's Bank. Tidal mixing also generated vertically mixed regions along the coast of the GOM, though as discussed

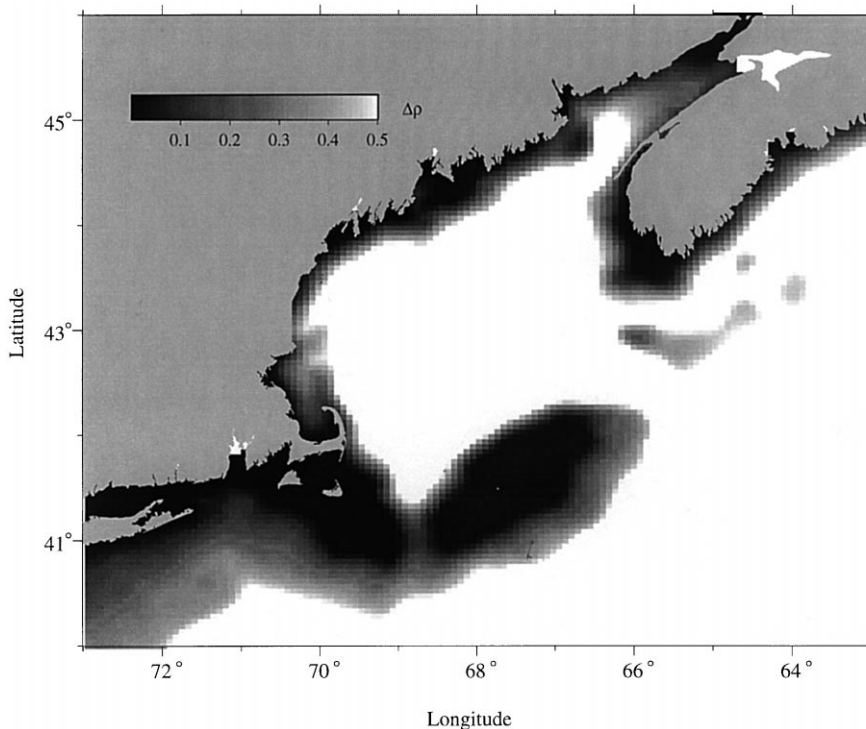


Fig. 4. Map of predicted top-to-bottom density difference averaged over the 20th tidal cycle.

below, these regions are influenced by wind and freshwater flow which are not included in the present version of the model.

The stratified and well-mixed waters were separated by tidal fronts of varying width. The fronts were very strong and narrow over the northern flank of GB, but broader over its southern flank. The tidal fronts were also relatively strong along the eastern edge of the NS, southeast of Cape Cod. The GB tidal fronts extended from the northern flank around the northeast peak, where they bifurcated; one front extended eastward, while the other tended southeast.

Details of the horizontal and vertical circulation patterns are thoroughly discussed in Chen et al. (2001).

5.2. Biological models

Case 1: Same as FC96.

As shown by FC96 (their Fig. 9), the surface, vertically integrated and peak phytoplankton biomasses off the bank were overestimated by about a factor of 2 using the original biological

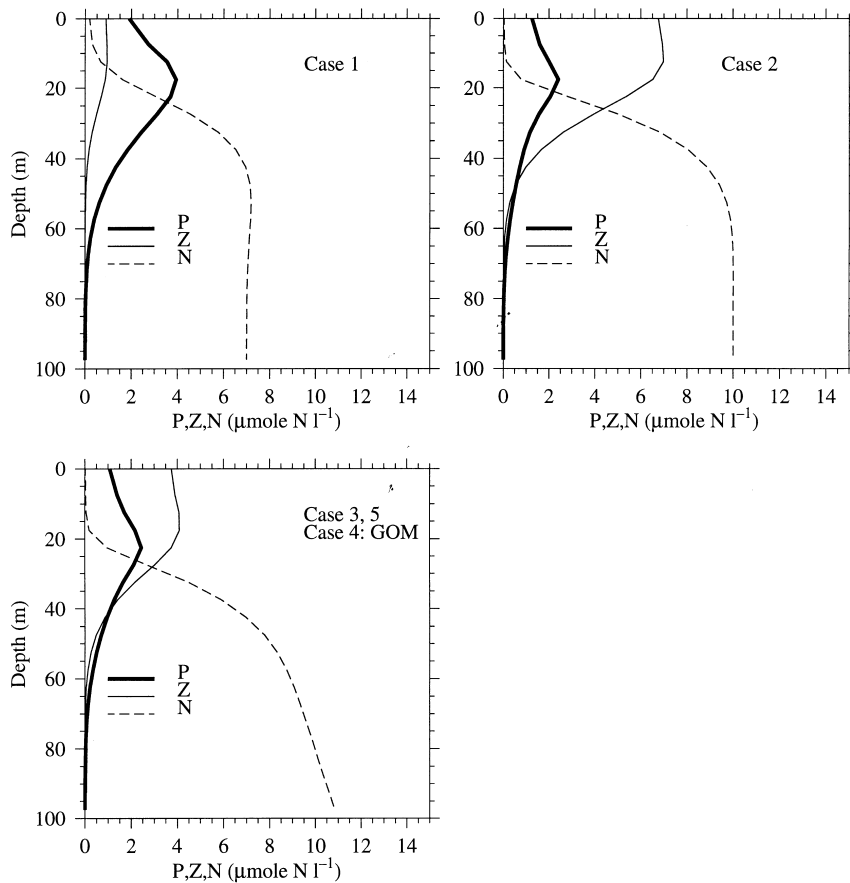


Fig. 5. Biological profiles from model grid points in the central GOM-averaged over the 20th tidal cycle.

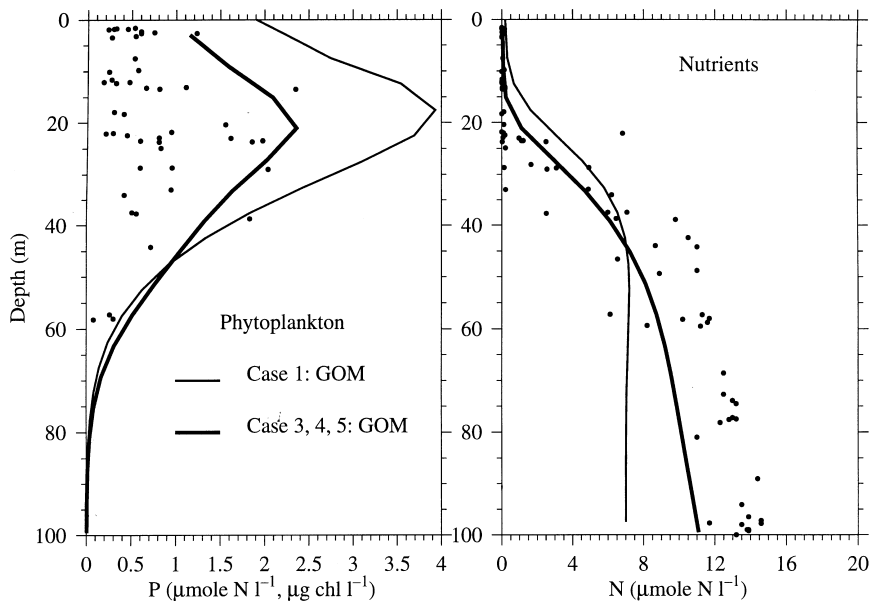


Fig. 6. Vertical profiles of phytoplankton (left panel) and nutrients (right panel) from Case 1 and Cases 3–5, compared to data from the central GOM (Townsend and Christensen, 1986, stations 01, 21, 22, 43, 44, 88, 89, 90, 91, B5, B7). Model profiles are averaged over the 20th tidal cycle.

parameter set. To some extent, this must reflect the differing phytoplankton communities on and off the bank: GB waters tend to be dominated by diatoms and other larger phytoplankton, while the deeper waters of the GOM have a higher proportion of nanoplankton (e.g., O'Reilly et al., 1987). These smaller phytoplankton in the GOM presumably support a well-developed microheterotroph community which is tightly coupled to the growth of the primary producers. The lower phytoplankton biomass also contributes to a deeper euphotic zone in the GOM than on GB, with a deeper subsurface chlorophyll maximum layer (O'Reilly et al., 1987). None of these features of the GOM are well simulated using the GB biological parameter set (Figs. 5 and 6).

In the course of developing the 3D physical–biological model, we were interested in how well the 2D model solutions of FC96 compared to the full (though more poorly resolved) 3D model. Such a comparison is shown in Fig. 7, where a cross-bank section corresponding to the location of the FC96 grid (Fig. 1, Section A) is taken from the 3D model with the same biological parameters. The coarser vertical resolution of the 3D simulation is evident in comparing the 2D and 3D cross-bank sections: the biological fields are not as well resolved, leading to differences in biomasses and resolution of patches. Still, it can be seen that there is no substantive difference between the 2D and full 3D simulations, suggesting that the 2D model captured the essential dynamics. This point is echoed in the comparison of the physical models, which showed that the only important term not well simulated in the 2D model was the along-bank pressure gradient (Chen et al., 2001).

Cases 2, 3: Modified biological parameters, nutrient profile.

To reflect the higher proportion of smaller phytoplankton and zooplankton in the waters of the GOM, the half-saturation constant for nutrient uptake and the death rate of zooplankton were

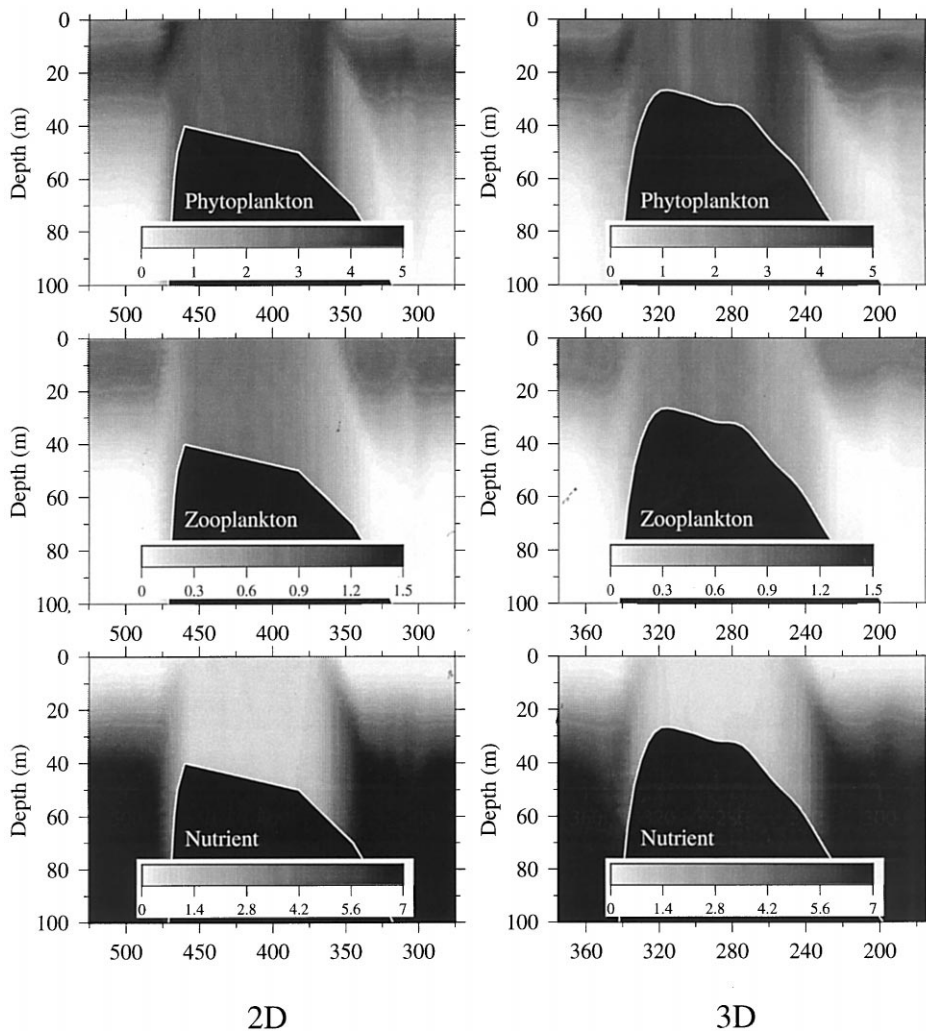


Fig. 7. Cross-bank sections from the 2D (FC96) and 3D (Case 1) models, both tidal averages over the 20th tidal cycle. Upper panels: phytoplankton, middle panels: zooplankton, lower panels: nutrients. Units: $\mu\text{mol N l}^{-1}$.

decreased (Table 1). The half-saturation constant is representative of smaller phytoplankton (e.g., Eppley et al., 1969), while the lower zooplanktonic death rate is assumed to better simulate the slower physiological decline of protists compared to crustaceans. A lower diffuse attenuation coefficient, k_{ext} , was used to simulate the clearer waters off the bank. The total amount of nutrient, N_T , was increased to reflect the high values of nitrate in the deep waters of the GOM.

The combination of these changes led to good agreement of the modelled phytoplankton and nutrient fields with data from the upper 30m of the GOM (Figs. 5 and 6). The subsurface chlorophyll maximum, a function of the phytoplankton growth and sinking rates, formed at about 20m, with a magnitude within those measured in the GOM (e.g. Townsend and Christensen, 1986;

Balch et al., 1991; Marra et al., 1993). The nutrient profile was also accurately reproduced, with a nutricline beginning around 20–25 m depth and undetectable nutrients in the surface waters (Townsend and Christensen, 1986; Christensen et al., 1996). While the depth of the nutricline is a little shallow in the model, it must be remembered that this model does not include wind forcing, which would tend to deepen and sharpen this feature.

The zooplankton biomass was predicted to be nearly $7 \mu\text{mol N l}^{-1}$ in the surface waters. Using appropriate conversions, Davis (1987) suggested values of about $1 \mu\text{mol N l}^{-1}$ for crustacean zooplankton, while Sambrotto and Langdon (1994) estimated about $3 \mu\text{mol N l}^{-1}$ for the micro-heterotrophs on GB, based on changes in oxygen, dissolved inorganic carbon, and nitrogen. Thus this model prediction for the zooplankton seems unreasonably high. In addition, the deeper nutrient concentrations are underestimated in the GOM. Christensen et al. (1996) show an almost linear increase of total inorganic nitrogen with depth below about 40 m depth, which is not captured by the model.

To improve the estimate of surface zooplankton and to obtain a better match with the deep nutrient distributions, a linear profile of total nutrient, N_T , was employed in the biological model initial condition (Case 3). The presumption is that surface nutrient values in summer are to some extent set by vertical mixing from deeper waters during winter (see Walsh et al., 1987). With an underlying vertical gradient of N_T , the total nitrogen in summertime surface waters would always be less than the highest values in the deep waters of the GOM. Using this vertical nutrient gradient, close agreement was obtained between the phytoplankton and nutrient profiles of the model and data (Figs. 5 and 6). The steady increase of dissolved nutrients with depth was accurately reproduced. The lower values of N_T in the surface waters led to lower zooplankton concentrations there, with predicted values of $3\text{--}4 \mu\text{mol N l}^{-1}$, consistent with observations (Davis, 1987; Sambrotto and Langdon, 1994).

Having obtained good agreement of vertical profiles of biological variables in the GOM, it is worthwhile exploring the horizontal distributions of biological properties across the model domain. A useful diagnostic field is the phytoplankton biomass, integrated to the bottom of the euphotic zone ($4.6/k_{\text{ext}}$) and averaged over a tidal period (Fig. 8). Note that Cases 2 and 3 have identical fields near the surface, thus only Case 3 is shown. In all the cases shown, the gross features are similar: high values of phytoplankton in the fronts surrounding GB, particularly on the northern flank of the bank. Phytoplankton concentration is also high along the east side of the NS and into the Great South Channel, with two zones of particularly high phytoplankton southeast of Cape Cod and southeast of Nantucket. These features are quite persistent, regardless of biological parameters or euphotic depths. The high phytoplankton biomass corresponds directly with regions of low stratification driven by tidal mixing (compare Fig. 8 with Fig 4). The high phytoplankton values in the GOM can be seen for Case 1, with lowered values using the Case 3 parameter set. The predicted phytoplankton concentrations agree well with data from the GB fronts and from the GOM.

One feature predicted by the Cases 1–3 models is a region of low phytoplankton concentration in the shallowest waters on the top of GB. The model predictions of $\sim 1.5 \mu\text{mol N l}^{-1}$ are low compared to values of 2–3 found by Horne et al. (1989) for the well-mixed waters on GB. In Case 3, the low phytoplankton biomass on GB arises directly from the initial condition: the deep euphotic zone extends to the bottom in the shallow waters on the bank, and there is no vertical gradient of phytoplankton within the euphotic zone. When tidal forcing is applied, the strong vertical mixing

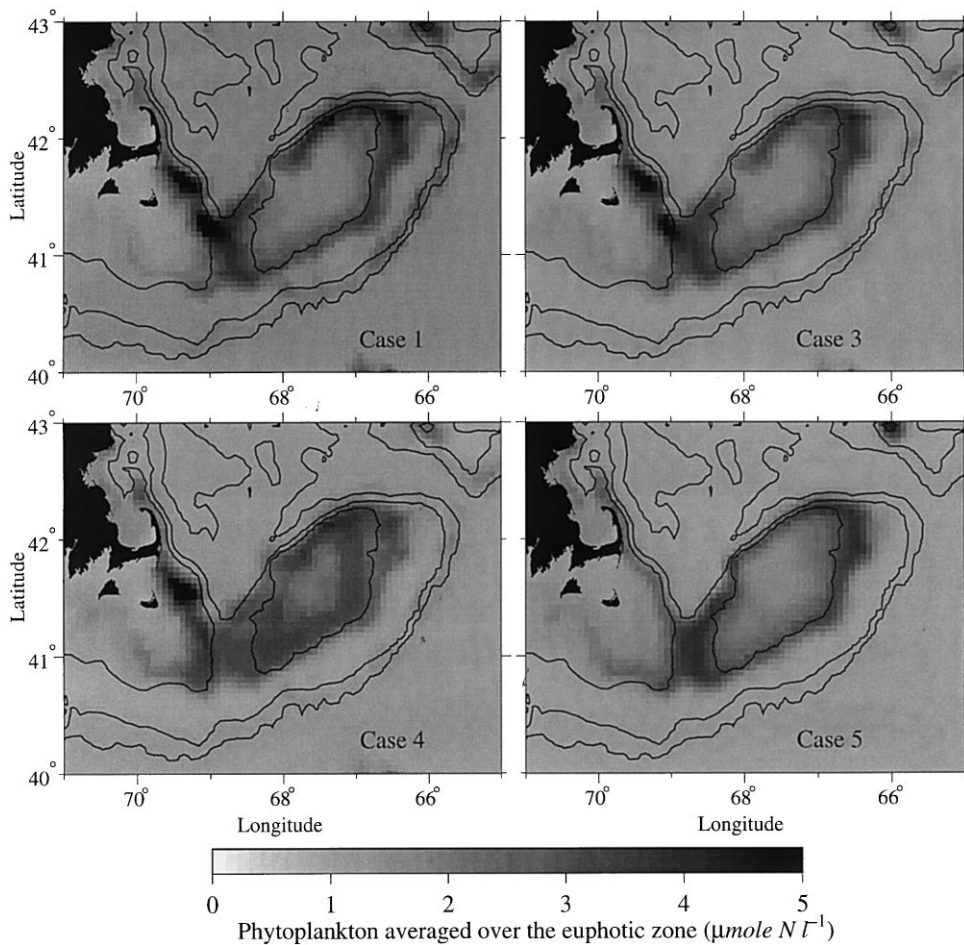


Fig. 8. Phytoplankton concentration averaged over the euphotic zone ($4.6/k_{\text{ext}}$) for Cases 1, 3–5, averaged over the 20th tidal cycle.

on the top of the bank homogenizes the initial condition, but does not affect the vertically homogeneous phytoplankton. The phytoplankton thus remain tightly coupled to the zooplankton as they were at the steady-state initial condition, and no growth of phytoplankton is seen. Given the fact that this low-biomass feature does not appear as strongly in most data from GB, we rejected Case 3 as a reasonable simulation of the full GB and GOM.

Case 4: Horizontally varying k_{ext} .

Given our strategy of changing only physical parameters after having achieved good agreement of the model in the GOM, one approach for obtaining better agreement of the modelled and observed phytoplankton biomass on GB is to reproduce the more shallow euphotic zone there. O'Reilly et al. (1987), for example, show euphotic depths of ~ 22 m on GB, but ~ 30 m in the GOM. The shallower euphotic depths on GB are presumably driven by elevated concentrations of phytoplankton and suspended material in those well-mixed waters. To explore the influence of

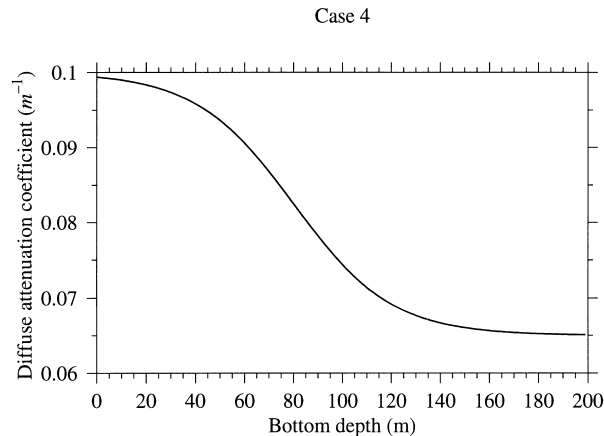


Fig. 9. Water-column depth-dependence of the diffuse attenuation coefficient, k_{ext} for Case 4.

shallower euphotic depths (higher k_{ext}) on GB, a horizontally varying k_{ext} was used whose value was low in deep waters, and increased as bottom depth decreased. A hyperbolic tangent function was used to smoothly interpolate k_{ext} between the deep and shallow waters (Fig. 9).

The model biological initial conditions using the horizontally variable k_{ext} show the phytoplankton to disappear below 45 m depth in the GOM, but to extend to only 33 m on GB (Fig. 3). This leaves a small pool of nutrients at the bottom on GB. This nutrient pool becomes homogenized as tidal mixing is imposed, and fuels further phytoplankton growth. The slow response time of the zooplankton allows the phytoplankton to grow with fewer grazing losses on GB, leading to increased phytoplankton biomasses on the central bank compared to the other cases (Fig. 8). The concentrations generated ($2\text{--}2.5 \mu\text{mol N l}^{-1}$), agree well with observations from GB ($\sim 2 \mu\text{g chl l}^{-1}$ in summer, e.g., O'Reilly et al., 1987; Horne et al. 1989).

The good agreement of the phytoplankton concentrations is well demonstrated by comparing the modelled tidal-average surface phytoplankton concentrations to satellite images of chlorophyll obtained during May and June of 1997 from the short-lived OCTS sensor (<http://seawifs.gsfc.nasa.gov/SEAWIFS.html>) (Fig. 10; note the logarithmic pigment scale). The agreement of biomass and location of features is striking: the high concentrations predicted south of Cape Cod are seen in the images; the high biomass within the 60 m isobath of GB is well reproduced, including its asymmetric shape and higher concentrations on the northeast peak; the line of high biomass predicted to the east of GB between the 100–200 m isobaths is also seen in the images; and the trail of phytoplankton tending westward along the mid-Atlantic Bight south of Cape Cod is accurately reproduced. The model does not reproduce the high concentrations along the coastal GOM. This nearshore band is driven more by river runoff and other nearshore nutrient sources than by tidal dynamics, suggesting that a more accurate simulation of the GOM requires the inclusion of freshwater runoff and its concomitant nutrient input. A further feature of the satellite images is the strong temporal variability: the high biomass present on GB from May 28 to June 9 is almost erased by June 11, indicating variability of forcing not included in the model.

Further agreement of the model and data can be found in comparing the cross-frontal distributions of nutrients and phytoplankton from the model Section B (Fig. 1) to the northern transect of

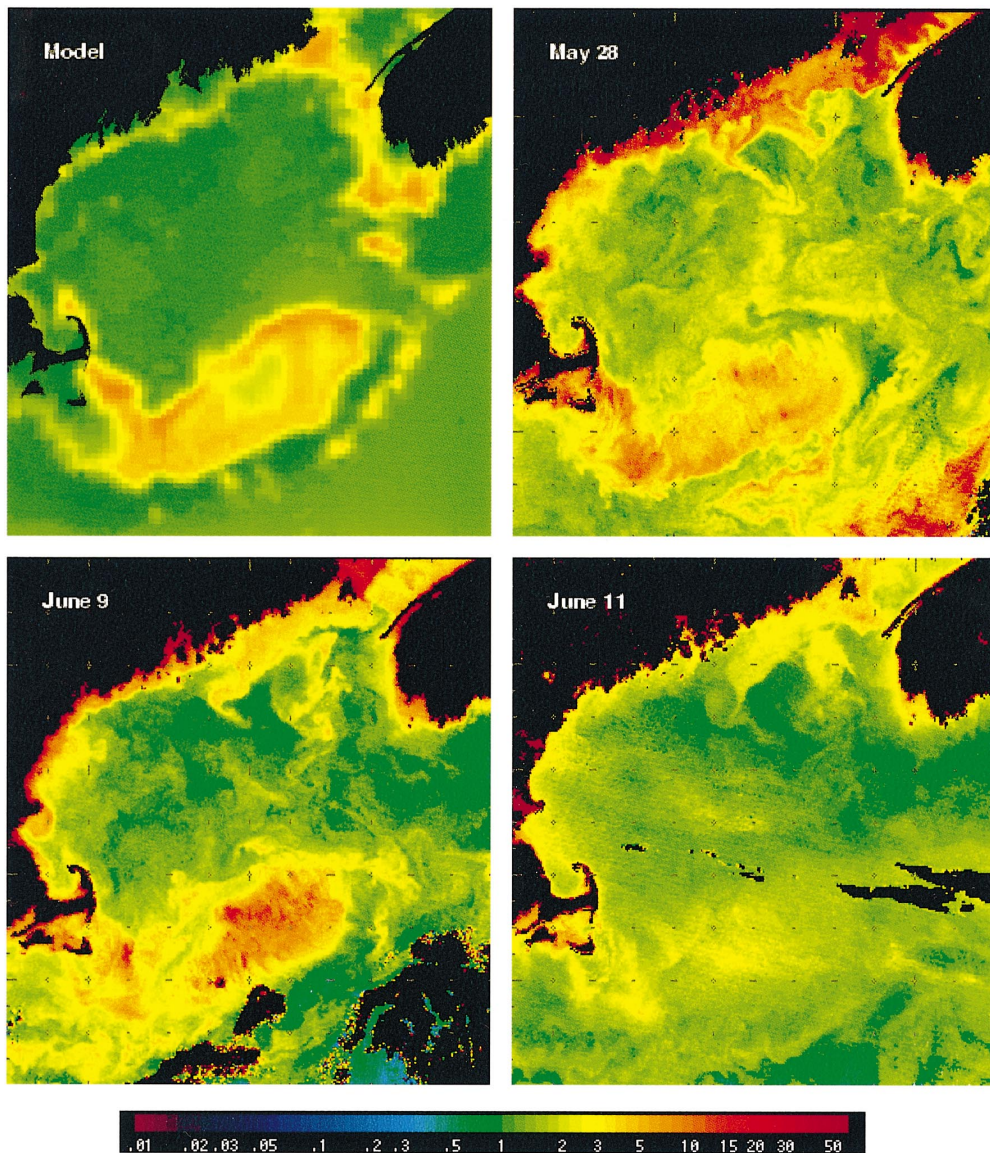


Fig. 10. Case 4 surface phytoplankton distributions ($\mu\text{mol N l}^{-1}$) averaged over the 20th tidal cycle (upper left) compared to OCTS images of chlorophyll from May 28 (upper right), June 9 (lower left) and June 11 (lower right) of 1997. Note the logarithmic color scale ($\mu\text{g chl l}^{-1}$).

Horne et al. (1989; their stations 295–302) (Fig. 11). The model resolution along this transect is approximately the same as the station spacing of Horne et al. The model field was chosen to correspond roughly to the same tidal phase as the Horne et al. transect (though the model field is one time step (not a tidal average), while the field transect took several hours to complete). The model nutrient isopleths have the same shape, and intersect the bottom at the same position on the

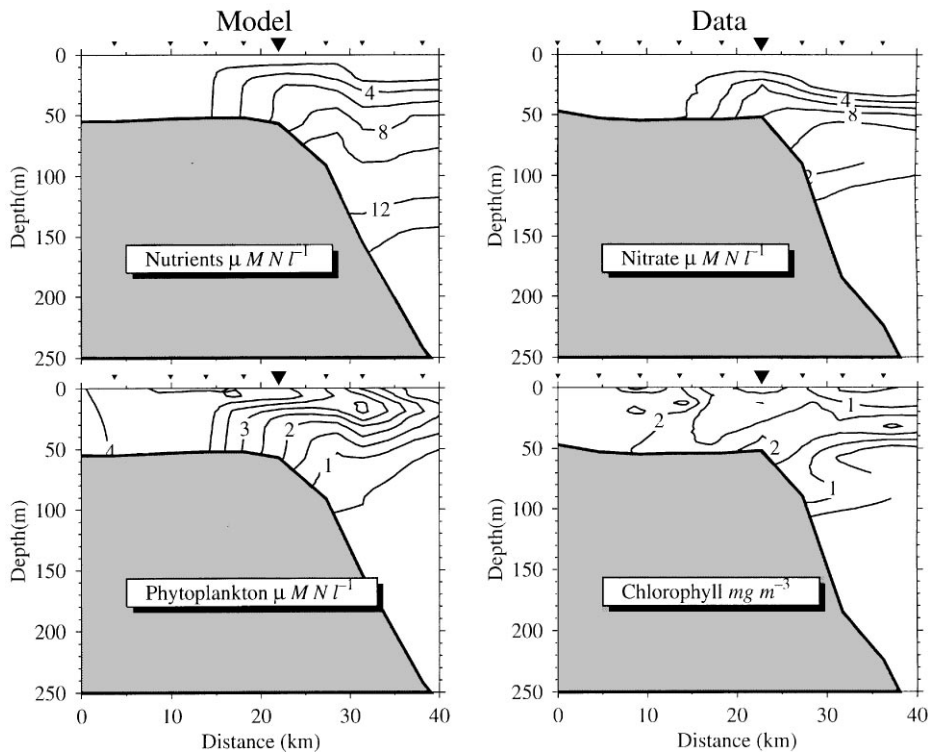


Fig. 11. Comparison of the model to data collected along Section B (Fig. 1). Upper panels: dissolved nutrients/nitrate $\mu\text{mol N l}^{-1}$. Lower panels: phytoplankton/chlorophyll ($\mu\text{mol N l}^{-1}$; $\mu\text{g l}^{-1}$). Left panels: model, right panels: data from Horne et al. (1989), stations 295–302. Triangles indicate station locations. Large triangle shows location of mooring station data in Fig. 12. Model fields are a single time point in the 20th tidal cycle (not an average).

bank as the field data. The model concentrations are higher near the surface than the data, and the nutricline is more diffuse. To some extent, this is a function of the low model resolution, and the vertical distributions of Fig. 6 from the GOM show the same tendency. The agreement is less good with the phytoplankton fields, though some of the trends are similar: higher values on the bank, where the phytoplankton are well mixed, and a subsurface maximum at 20–30 m depth (deeper in the data than the model) off the bank. The model concentrations are almost twice as high as the data on the bank, though field samples collected a week earlier (see below) give phytoplankton concentrations up to $6 \mu\text{g l}^{-1}$ in this same area, indicating a degree of temporal and spatial patchiness not captured in the model.

Modelled nutrient and phytoplankton fields also show good agreement with time/depth-series data from a mooring deployed by Horne et al. (1989; their stations 170–192) (Fig. 12). There was no model grid point corresponding exactly to the mooring location. The strong horizontal gradients of biological properties in this frontal region mean that small discrepancies in location result in large differences in concentrations over a tidal cycle. Nevertheless, the qualitative and quantitative agreement of the modelled and measured nutrient and phytoplankton fields from nearby points is

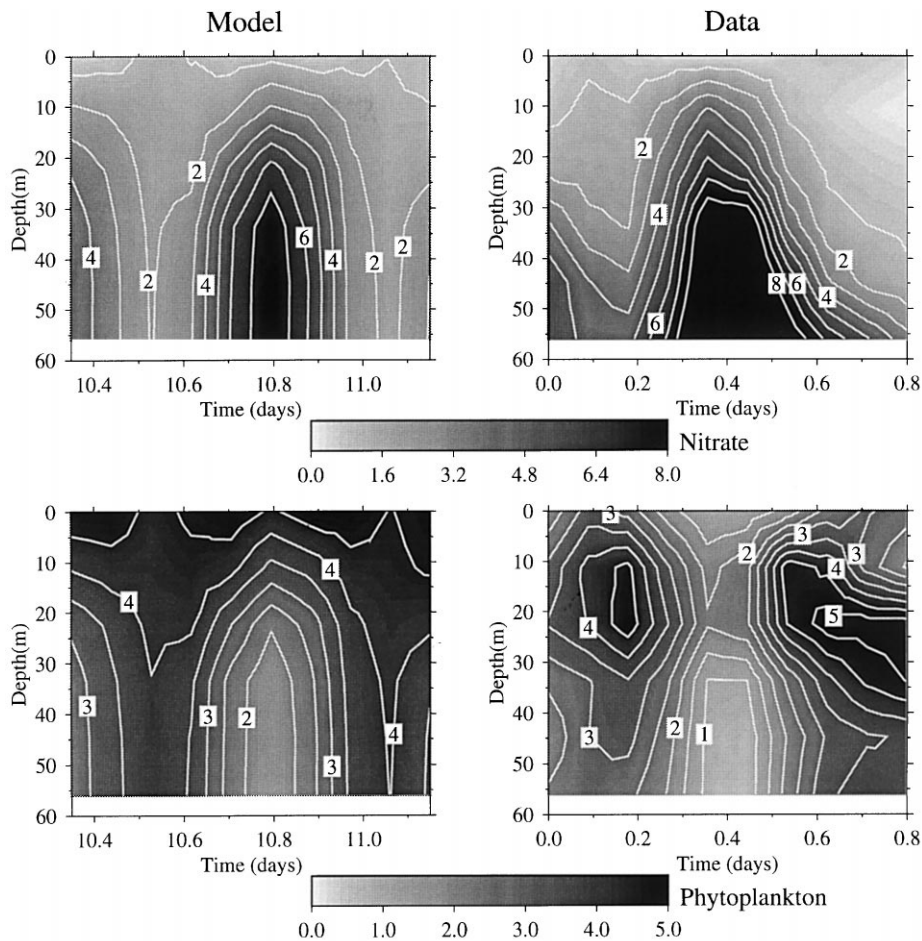


Fig. 12. Comparison of model to data collected at the mooring station indicated in Fig. 11 (large triangle). Upper panels: dissolved nutrients/nitrate ($\mu\text{mol N l}^{-1}$). Lower panels: phytoplankton/chlorophyll ($\mu\text{mol N l}^{-1}$; $\mu\text{g l}^{-1}$). Left panels: model, right panels: data from Horne et al. (1989) stations 170–192. The model has been subsampled at approximately the same frequency as the data.

encouraging. The strong on-bank flux of nutrients during the on-bank phase of the tidal motions is evident in both the model and data fields, though the data showed higher concentrations near the bottom as the deep nutrient pool was advected up the flank of the bank. The high nutrient concentrations correspond to low phytoplankton concentrations in both the model and data. The model and data phytoplankton concentrations show better agreement than in the transect data (Fig. 11), particularly below 10 m depth. Note that the mooring location was almost the same location as one of the transect stations of Fig. 11, but was sampled a week earlier, again indicating the strong temporal variability of the biological fields on GB. The modelled and measured phytoplankton fields show the poorest agreement in the upper 10 m, where the model

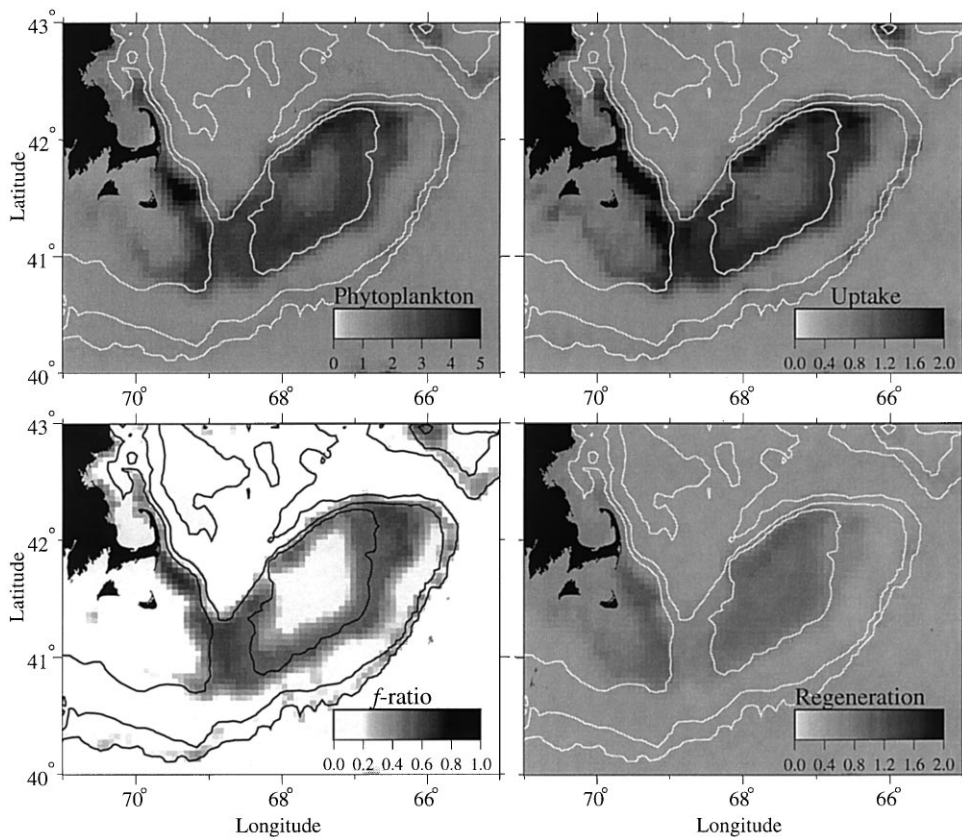


Fig. 13. Case 4: Phytoplankton ($\mu\text{mol N l}^{-1}$), uptake rate ($\mu\text{mol N l}^{-1} \text{d}^{-1}$), f -ratio and regeneration rate ($\mu\text{mol N l}^{-1} \text{d}^{-1}$) averaged over the euphotic zone ($4.6/k_{\text{ext}}$), and over the 20th tidal cycle.

overestimates the concentrations. Again, the model does not include any upper-ocean forcing (heat flux or wind stress), limiting its ability to recreate the biological patterns in those waters.

Given the generally good agreement of the phytoplankton and nutrient fields in the GOM and on GB for Case 4, it is worth exploring the dynamics in more detail. Comparing Fig. 10 with Fig. 4 it can be seen that the areas of high phytoplankton concentration correspond well to regions of strong tidal mixing. In these regions, uptake of nutrients by phytoplankton integrated over the euphotic zone exceeds the regeneration of nutrients by zooplankton (Fig. 13). Though the model cannot distinguish “new” and “recycled” production (sensu Dugdale and Goering, 1967; Eppley and Peterson, 1979), we can calculate an f -ratio based on the uptake of nutrients by phytoplankton *not* accounted for by recycled nutrients from the zooplankton ($f = [\text{uptake} - \text{regeneration}] / \text{uptake}$). This ratio varies between zero and one, with high values indicating a high proportion of primary production supported by nutrients other than those supplied through recycling. From Fig. 13, it can be seen that the areas of high phytoplankton biomass surrounding GB and the NS are also areas of high f -ratio. As we will see when comparing Cases 3–5 (no advection) most of the nutrients

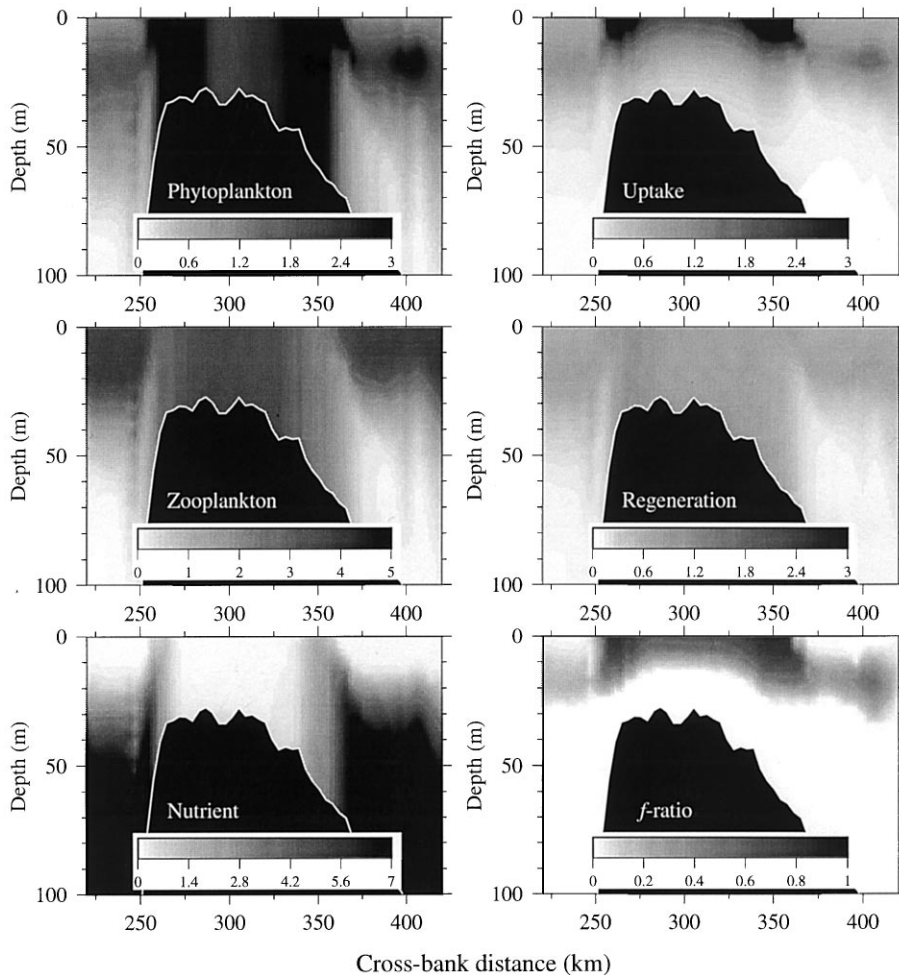


Fig. 14. Case 4: Vertical section across GB. Left-hand panels: top, phytoplankton ($\mu\text{mol N l}^{-1}$); middle, zooplankton ($\mu\text{mol N l}^{-1}$); bottom, nutrients ($\mu\text{mol N l}^{-1}$). Right-hand panels: top, uptake rate ($\mu\text{mol N l}^{-1} \text{d}^{-1}$); middle, regeneration rate ($\mu\text{mol N l}^{-1} \text{d}^{-1}$); bottom, f -ratio. Averages over the 20th tidal cycle.

fueling the high f -ratios in these regions of high phytoplankton biomass are delivered through advective processes, emphasizing the importance of including 2D and 3D dynamics when modeling biological systems in strongly forced, topographically complex areas.

A section across GB reveals patterns similar to those described by FC96: a patch of high phytoplankton in the tidal front on the northern flank of GB, tongues of high-nutrient water extending toward the euphotic zone at the fronts on the southern and northern flanks, and regions of high f -ratio in the frontal waters (Fig. 14). These patterns correspond qualitatively and quantitatively to those observed by Horne et al. (1989, 1996) on GB. The sinking of the phytoplankton leads to a subsurface chlorophyll maximum at about 20 m (see also Figs. 6, 11 and 12), and a weak cross-frontal nutrient flux drives the phytoplankton patch in the northern front. Vertical

mixing on GB leads to the phytoplankton seeing an average light level over the water column, though uptake is restricted to the surface waters, as this process is coupled to irradiance. On the top of GB, vertically integrated uptake is balanced by regeneration of nutrients by zooplankton, indicating the close coupling of primary and secondary production in these waters (and therefore low f -ratios). Horne et al. (1989) found f ratios up to 0.7 in the frontal waters of GB, while Sathyendranath et al. calculated values of ~ 0.55 , both similar to those calculated here. Our predicted values of ~ 0.1 in the GOM are lower than the Horne et al. values of ~ 0.3 , or the Sathyendranath et al. values of 0.27–0.4, suggesting a tighter trophic coupling in the model than in the GOM. The addition of wind and heat fluxes would tend to weaken this coupling, leading to higher f -ratios in the modelled GOM. Our modelled surface phytoplankton concentrations of $\sim 1 \mu\text{mol N l}^{-1}$ in the GOM, and a subsurface peak of $\sim 2 \mu\text{mol N l}^{-1}$ agree with Horne et al.'s measurements off GB, though our predicted surface concentrations tend to be slightly higher than their observations. The predicted frontal concentrations of 3.5–4.5 $\mu\text{mol N l}^{-1}$ agree with the chlorophyll measurements of 2–5 $\mu\text{g chl l}^{-1}$ made by Horne et al., though they are slightly higher than the 1.5–2.8 $\mu\text{g chl l}^{-1}$ estimated by Sathyendranath et al. Our modelled on-bank concentrations of 2–3 $\mu\text{mol N l}^{-1}$ are similar to the values $< 2 \mu\text{g chl l}^{-1}$ found by Horne et al., but lower than the values of 3.8–5.4 $\mu\text{g chl l}^{-1}$ reported by Sathyendranath et al. Overall, we find good agreement of the modelled and observed plankton concentrations, and feel that this model is an adequate representation of the basic biological processes occurring in this region.

Case 5: No advection of biology.

Several models have attempted to simulate the primary production in tidal fronts using 1D (vertical) models with turbulent mixing (e.g., Tett, 1981; Sharples and Tett, 1994). To assess whether such models are adequate, and to address the contribution of advection to the simulated patterns in our 3D model, we removed advection from the 3D biological model (Case 3). The physical model operated as before, with the full range of physical processes, however, the biological components were forced only with the vertical mixing generated by the physical model — there was no horizontal exchange of biological materials between the model grid points. The biological model thus acted like an array of horizontally uncoupled vertical 1D models. To obviate the effect of the horizontally varying k_{ext} , this case was run with the same parameters as Case 3 (i.e. no horizontal dependence of k_{ext}), and so will be compared with Case 3.

The phytoplankton fields in Fig. 8 show only small differences between the full 3D simulation (Case 3) and Case 5 (no advection). The width of the frontal zone is higher in Case 3, due to the cross-isobath migration of the frontal zone with the tides — the tidal-averaging smears this feature over a broader range in Case 3. The high biomass south of Cape Cod is not generated without advection, while a region of high biomass appears in the Great South Channel in the no-advection case that is not apparent in Case 3. The patches of phytoplankton between the 100 and 200 m isobaths on the southern flank of GB are not generated without advection, though the patch on Brown's Bank is stronger without advection.

A clue to the importance of these differences lies in the maps of the f -ratio (Fig. 15). The relatively broad areas of high (> 0.5) f -ratio in Case 3 are reduced to narrow bands or eliminated in Case 5. This implies that the delivery of nutrients from below the euphotic zone is suppressed when advection is removed. Advection also spreads the developing phytoplankton patches away from their origin, leading to an increased area of high phytoplankton biomass in the simulation with advection (Case 3).

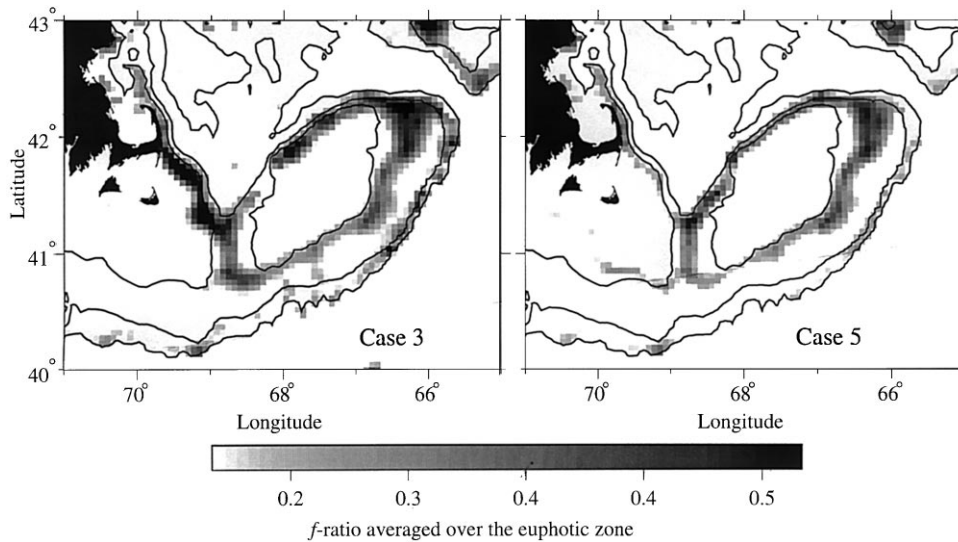


Fig. 15. Comparison of f -ratio averaged over the euphotic zone for Cases 3 and 5 (no advection), averaged over the 20th tidal cycle.

In spite of these differences, the no-advection case (Case 5) gave a surprisingly good simulation of the patterns in the GOM and on GB. The vertical profiles of properties were quite similar to those of Case 3, including the subsurface patches of phytoplankton in the tidal fronts on GB, and the tongues of high nutrient extending into the euphotic zone at the fronts (not shown).

6. Discussion

We have presented a fully 3D physical–ecosystem model of the Gulf of Maine and Georges Bank. All the biological parameterizations used gave reasonable qualitative simulations of the gross features in the GOM and on GB: high phytoplankton biomass in the tidal fronts surrounding GB, and the eastern edge of the NS; a subsurface chlorophyll maximum layer in the GOM at about 20 m, corresponding to the depth of the nutricline; high f -ratios in the frontal waters of GB; and a line of high phytoplankton biomass between the 100 and 200 m isobaths on the eastern side of GB. With some modification of the biological parameters, excellent quantitative fits were obtained of the predicted phytoplankton and nutrient profiles with data from the GOM. Quantitative agreement was also found between predicted phytoplankton patterns and satellite images of pigment distributions in this region.

Our strategy in performing this modelling was to set the biological parameters so that a good fit was obtained with data from the GOM, and then compare the GB predictions to data. In this sense, the predicted GB distributions were a perturbation of the GOM dynamics, forced by tidal mixing and advection on the bank. To answer the question posed earlier, it appears that the nutrients, phytoplankton and zooplankton on GB can be modelled adequately as a physical

perturbation of the GOM patterns. Improvement of the GB predictions was obtained if a horizontally variable diffuse attenuation coefficient was used, indicating the importance of spatial variations in the euphotic depth in controlling biological patterns in coastal regions.

Even the worst cases of this model gave reasonable qualitative agreement with the observed patterns in the GOM and on GB, suggesting that this simple NPZ model is quite robust to changes in parameter values. More importantly, it implies that the patterns of nutrients and phytoplankton, in particular, are strongly determined by tidal mixing in the GOM and on GB. This is no surprise, given the wealth of field work supporting this contention. However, it was surprising how persistent the patterns of phytoplankton and nutrients were around GB, in spite of some large changes in biological parameter values (including other cases not presented here). Clearly, tidally forced vertical mixing is the predominant determinant of biological structures around GB.

Comparison of the predicted phytoplankton patterns with satellite images showed good agreement in the GOM and on GB, but poor agreement in the nearshore coastal regions of the GOM. It is likely that the underprediction of coastal pigment levels is due to the lack of freshwater (and therefore nutrient) inflows along the coast in the model. The presence of several large rivers in Maine, New Hampshire and Massachusetts contributes strongly to the nearshore nutrient budget (e.g., Townsend et al., 1987). Benthic fluxes of nutrients also may play a role in supporting high phytoplankton biomass in the nearshore regions, a process not included in the present model.

The simulated nutrient profiles agreed well with data from the GOM, though the nutricline tended to be a little shallow and diffuse in the model. The model was forced only with tides; the inclusion of wind forcing and a diel heat flux would tend to deepen and sharpen the nutricline, leading to better agreement between model and data.

The good comparison between model and data on GB suggests that changes in biological fields on the bank are largely due to tidal forcing. This forcing is manifested as mixing and advection. Mixing appears to be the most biologically important of these two forcings, given the results of the no-advection simulation (Case 5). The cross-bank patterns of phytoplankton and nutrients were not substantially changed from the case with advection (Case 3) — even the phytoplankton patches in the tidal fronts were generated with only a temporally varying vertical mixing. Advection, however, is critical to maintaining cross-frontal fluxes of nutrients (and other properties), as indicated by the low f -ratios in the no-advection case. The implication is that long-term simulations of biological dynamics on GB must include 2D and 3D dynamics, while shorter-term simulations may be adequately represented using a detailed model of vertical mixing.

Georges Bank has some of the highest levels of primary production of any shelf ecosystem in the world (O'Reilly et al., 1987; Cohen and Grosslein, 1987). Studies employing a variety of methods have given the summertime productivity at $\sim 2 \text{ gC m}^{-2} \text{ d}^{-1}$ in the well-mixed waters of GB, and about half that in the GOM (Hopkins and Garfield, 1981; Horne et al., 1989; Sathyendranath et al., 1991). At a grid point on the top of the bank, our model predicts $1.8 \text{ gC m}^{-2} \text{ d}^{-1}$, indistinguishable from the data. However, when the model data are integrated over all the well-mixed waters of GB (defined as a surface-to-bottom temperature difference of $< 0.1^\circ\text{C}$), we obtain $\sim 4 \text{ gC m}^{-2} \text{ d}^{-1}$ for all cases (range 3.8–4.2). As suggested by FC96 and Horne et al. (1989), this indicates that a high proportion of the production on GB occurs in the waters just inshore of the tidal fronts — waters that may be unstratified on average, but have a tidal cycle to their stratification. This estimate of production is twice the synoptic estimate of Sathyendranath et al. (1991) who used compound remote sensing to calculate primary and new production on the bank. While the simplicity of our

biological model suggests that we view the estimate of $4 \text{ gC m}^{-2} \text{ d}^{-1}$ with some skepticism, it does suggest that we require better spatial resolution of primary production estimates from the tidally forced waters of GB.

The modified biological parameter sets (Cases 2–5) were more representative of smaller phytoplankton and their microheterotrophic grazers in the GOM. These small plankton tend to dominate in the GOM, both in biomass and in their contribution to primary productivity (e.g., O'Reilly et al., 1987). Their dominance is decreased on GB, where strong physical forcing and nutrient supply from deeper waters favors a higher concentration of large phytoplankton, particularly diatoms. This shift in the size structure of the primary producers, and consequent changes in the grazer community cannot be captured with such a simple biological model. In particular, the crustacean zooplankton are probably not well simulated by this model, given their long generation times and complicated life histories. Better agreement between model and data might be obtained with a more highly resolved biological model, including at least two size classes of phytoplankton, and two size classes of zooplankton. One of the main impediments to employing such a model is the dearth of appropriate data with which to initialize and test the model. Though we did not by any means conduct an exhaustive literature review, it was difficult to find data on the nitrogen content and distribution patterns of the microheterotrophs on GB and in the GOM. Data of this type being gathered by the US GLOBEC program should help fill this gap.

The patterns of primary production and new production predicted by the various cases of the model were surprisingly robust. Even the removal of advection left patches of high new and primary production along the northern flank of GB, on the northeast peak of GB, and to some extent along the eastern flank of the NS. The stability of these patterns suggests a fundamental response of the plankton to the local physical forcing, leading to elevated production. It is probably no coincidence that these areas are also important for several commercially relevant fish and invertebrate species. Tremblay and Sinclair (1992) and Thouzeau et al. (1991) showed the northeast peak of GB to have extensive scallop (*Placopecten magellanicus*) beds between the 60 and 100 m isobaths. Tremblay and Sinclair's October cruises also showed high abundances of scallop larvae associated with the tidal fronts in that area. Juvenile cod (*Gadus morhua*) and haddock (*Melanogrammus aeglefinus*) also were found to be concentrated in these waters on the northeast peak of GB (Lough et al., 1989). Polacheck et al. (1992) found high concentrations of haddock eggs near the northeast peak of GB in the late spring/early summer of 1987, though the unusually high freshwater runoff of that year led to unusual circulation patterns in the GOM. Wigley and Serchuch (1992) showed the highest spring and autumn concentrations of juvenile cod to occur almost precisely where the present model (Case 4) predicted the highest primary production and *f*-ratios: the eastern flank of the NS, and the northern and northeastern flanks of GB. Similarly, Sinclair and Isles (1985) showed two main spawning areas of Atlantic herring (*Clupea harengus*) to be along the eastern flank of the NS and along the northern flank of GB. The strong coincidence of the simulated regions of high new and primary production with the spawning grounds of many fish and invertebrate species suggests that the local physically mediated biological conditions are sufficiently predictable and evolutionarily favorable to offset the expenses of reproduction and growth.

The physical–biological model presented here is a first step in developing a basic physical/ecosystem model of the GOM and GB. Our model gives a reasonable representation of the planktonic and nutrient fields during summer in this region. Clearly, a great deal of biological

detail is lacking in this model, including any representation of size structure in the plankton, and the two dominant nitrogen sources in the region: ammonium and nitrate. The model forcing is extremely simple: nothing but the topography and the M2 tide. The model, now, must be made more realistic with the addition of a more detailed biological model, wind forcing, heat flux variations, and freshwater inputs. Ultimately, we hope to have a model that will give accurate seasonal and annual cycles of planktonic fields in the GOM and on GB. This must proceed in increments, however, with studies of the dynamics of a more complicated plankton model, and the short-term response of the coupled models to wind, diel heat flux, and neap-spring variations of the tidal forcing.

Acknowledgements

Many thanks to Ed Horne, John Loder and David Townsend for supplying their field data and allowing us to use it. We thank Hui Tian for running several of these simulations, and Jamie Pringle for useful discussions. Comments from two anonymous reviewers hopefully improved the quality of the manuscript. This work was supported by the US GLOBEC program through NOAA Grant NA76GP0176 to PJSF, and NOAA Grant NA56RG0487 to CC. This is US GLOBEC contribution number 148.

References

- Balch, W.M., Holligan, P.M., Ackleson, S.G., Voss, K.J., 1991. Biological and optical properties of mesoscale coccolithophore blooms in the Gulf of Maine. *Limnology and Oceanography* 36, 629–643.
- Blumberg, A.F., 1994. A primer of ECOM3D-si. Technical Report, HydroQual, Inc. Mahwah, NJ, 84 pp.
- Blumberg, A.F., Mellor, G.L., 1987. A description of a three-dimensional coastal ocean circulation model. In: N.S. Heaps (Ed.), “Three-Dimensional Coastal Ocean Models”, *Coastal and Estuarine Science* 4, 1–16.
- Chen, C., Beardsley, R.C., Franks, P.J.S., 2001. A 3-D prognostic numerical model study of the Georges Bank ecosystem. Part I: physical model. *Deep-Sea Research II* 48, 419–456.
- Christensen, J.P., Townsend, D.W., Montoya, J.P., 1996. Water column nutrients and sedimentary denitrification in the Gulf of Maine. *Continental Shelf Research* 16, 489–515.
- Cohen, E.B., Grosslein, M.D., 1987. Production on Georges Bank compared with other shelf ecosystems. In: Backus, R.H. (Ed.), “Georges Bank”. The MIT Press, Cambridge, MA, pp. 383–391.
- Davis, C.S., 1987. Zooplankton life cycles. In: Backus, R.H. (Ed.), “Georges Bank”. The MIT Press, Cambridge, MA, pp. 256–267.
- Dugdale, R.C., Goering, J.J., 1967. Uptake of new and regenerated forms of nitrogen in primary productivity. *Limnology and Oceanography* 12, 196–206.
- Egbert, G.D., Bennett, A.F., Foreman, M.G.G., 1994. TOPEX/POSEIDON tides estimated using a global inverse model. *Journal of Geophysical Research* 99, 24821–24852.
- Eppley, R.W., Peterson, B.J., 1979. Particulate organic matter flux and planktonic new production in the deep ocean. *Nature* 282, 677–680.
- Eppley, R.W., Rogers, J.N., McCarthy, J.J., 1969. Half-saturation constants for uptake of nitrate and ammonium by marine phytoplankton. *Limnology and Oceanography* 14, 912–920.
- Franks, P.J.S., Chen, C., 1996. Plankton production in tidal fronts: a model of Georges Bank in summer. *Journal of Marine Research* 54, 631–651.

- Franks, P.J.S., Wroblewski, J.S., Flierl, G.R., 1986. Behavior of a simple plankton model with food-level acclimation by herbivores. *Marine Biology* 91, 121–129.
- Galperin, B., Kantha, L.H., Hassid, S., Rosati, A., 1988. A quasi-equilibrium turbulent energy model for geophysical flows. *Journal of Atmospheric Science* 45, 55–62.
- Hopkins, T.S., Garfield III, N., 1981. Physical origins of Georges Bank water. *Journal of Marine Research* 39, 465–500.
- Horne, E.P.W., Loder, J.W., Harrison, W.G., Mohn, R., Lewis, M.R., Irwin, B., Platt, T., 1989. Nitrate supply and demand at the Georges Bank tidal front. *Scientia Marina* 53, 145–158.
- Horne, E.P.W., Loder, J.W., Naimie, C.E., Oakey, N.S., 1996. Turbulence dissipation rates and nitrate supply in the upper water column on Georges Bank. *Deep-Sea Research II* 43, 1683–1712.
- Klein, P., 1987. A simulation of some physical and biologic interactions. In: Backus, R.H. (Ed.), “Georges Bank”. The MIT Press, Cambridge, MA, pp. 395–402.
- Kurlansky, M., 1998. *Cod: a Biography of the Fish that Changed the World*. Penguin, USA. 304.
- Lewis, C.V., Davis, C.S., Gawarkiewicz, G., 1994. Wind-forced biological-physical interactions on an isolated off-shore bank. *Deep-Sea Research II* 41, 51–73.
- Lough, R.G., Valentine, P.C., Potter, D.C., Auditore, P.J., Bolz, G.R., Neilson, J.D., Perry, R.I., 1989. Ecology and distribution of juvenile cod and haddock in relation to sediment type and bottom currents on eastern Georges Bank. *Marine Ecology Progress Series* 56, 1–12.
- Lynch, D.R., Gentleman, W.C., McGillicuddy, Jr., D.J., Davis, C.S., 1998. Biological/physical simulations of *Calanus finmarchicus* population dynamics in the Gulf of Maine. *Marine Ecology Progress Series* 169, 189–210.
- Marra, J., Chamberlin, W.S., Knudson, C., 1993. Proportionality between in situ carbon assimilation and bio-optical measures of primary production in the Gulf of Maine in summer. *Limnology and Oceanography* 38, 232–238.
- Mellor, G.L., Yamada, T., 1974. A hierarchy of turbulence closure models for planetary boundary layers. *Journal of Atmospheric Science* 33, 1791–1896.
- Mellor, G.L., Yamada, T., 1982. Development of a turbulence closure model for geophysical fluid problems. *Reviews of Geophysics and Space Physics* 20, 851–875.
- O’Reilly, J.E., Evans-Zetlin, C., Busch, D.A., 1987. Primary production. In: Backus, R.H. (Ed.), “Georges Bank”. The MIT Press, Cambridge, MA, pp. 220–233.
- Polacheck, T., Mountain, D., McMillian, D., Smith, W., Berrien, P., 1992. Recruitment of the 1987 year class of Georges Bank haddock (*Melanogrammus aeglefinus*): the influence of unusual larval transport. *Canadian Journal of Fisheries and Aquatic Sciences* 49, 484–496.
- Sambrotto, R.N., Langdon, C., 1994. Water column dynamics of dissolved inorganic carbon (DIC), nitrogen and O₂ on Georges Bank during April, 1990. *Continental Shelf Research* 14, 765–789.
- Sathyendranath, S., Platt, T., Horne, E.P.W., Harrison, W.G., Ulloa, O., Outerbridge, R., Hoepffner, N., 1991. Estimation of new production in the ocean by compound remote sensing. *Nature* 353, 129–133.
- Sharples, J., Tett, P., 1994. Modelling the effect of physical variability on the midwater chlorophyll maximum. *Journal of Marine Research* 52, 219–238.
- Sinclair, M., Isles, T.D., 1985. Atlantic herring (*Clupea harangus*) distributions in the Gulf of Maine-Scotian Shelf area in relation to oceanographic features. *Canadian Journal of Fisheries and Aquatic Sciences* 42, 880–887.
- Tett, P., 1981. Modelling phytoplankton production at shelf–sea fronts. *Philosophical Transactions of the Royal Society of London A* 302, 605.
- Thouzeau, G., Robert, G., Smith, S.J., 1991. Spatial variability in distribution and growth of juvenile and adult sea scallops *Placopecten magellanicus* (Gemlin) on eastern Georges Bank (Northwest Atlantic). *Marine Ecology Progress Series* 74, 205–218.
- Townsend, D.W., Christensen, J.P., 1986. Summertime oceanographic conditions in the Gulf of Maine, 16–24 July, 1985: physical oceanographic, nutrient and chlorophyll data. Technical Rept. No. 62, Bigelow Laboratory for Ocean Sciences. 137.
- Townsend, D.W., Christensen, J.P., Stevenson, D.K., Graham, J.P., Chenoweth, S.B., 1987. The importance of a plume of tidally mixed water to the biological oceanography of the Gulf of Maine. *Journal of Marine Research* 45, 699–728.

- Tremblay, M.J., Sinclair, M., 1992. Planktonic sea scallop larvae (*Placopecten magellanicus*) in the Georges Bank region: broadscale distribution in relation to physical oceanography. *Canadian Journal of Fisheries and Aquatic Sciences* 49, 1597–1615.
- Walsh, J.J., Whitley, T.E., O'Reilly, J.E., Phoel, W.C., Draxler, A.F., 1987. Nitrogen cycling on Georges Bank and the New York Shelf: a comparison between well-mixed and seasonally stratified waters. In: Backus, R.H. (Ed.), "Georges Bank". The MIT Press, Cambridge, MA, pp. 234–246.
- Wigley, S.E., Serchuch, F.M., 1992. Spatial and temporal distribution of juvenile Atlantic cod *Gadus morhua* in the Georges Bank-Southern New England region. *Fisheries Bulletin* 90, 599–606.